


Received August 28, 2018, accepted September 13, 2018, date of publication September 18, 2018, date of current version October 12, 2018.

Digital Object Identifier 10.1109/ACCESS.2018.2870865

A Precise Harmonic Control Technique for High Efficiency Concurrent Dual-Band Continuous Class-F Power Amplifier

ZHENXING YANG¹, YAO YAO², MINGYU LI¹ , (Member, IEEE), YI JIN³, TIAN LI¹, ZHEN GEN¹, AND ZHIQIANG YU¹

¹School of Microelectronics and Communication Engineering, Chongqing University, Chongqing 400044, China

²School of Electronic Science and Engineering, University of Electronic Science and Technology of China, Chengdu 611731, China

³Xi'an Branch of the China Academy of Space Technology, Xi'an 710100, China

Corresponding author: Mingyu Li (myli@cqu.edu.cn)

This work was supported in part by the Youth Foundation of China High Resolution Earth Observation under Grant GFZX04061502, in part by the Fundamental Research Funds for the Central Universities under Grant 2018CDGFTX0015, and in part by the National Natural Science Foundation of China under Grant 61801377.

ABSTRACT In this paper, a design approach for a high-efficiency concurrent dual-band power amplifier (PA) with precise harmonic control up to third order is proposed. With the precise harmonic control approach, the high-efficiency performance of the PA can be improved at two arbitrary wide interval frequencies. Based on the inherent impedance matching flexibility of the continuous Class-F (CCF) operating mode, the design spaces of fundamental and harmonic impedances of the PA are largely expanded. The optimal impedances of a CCF PA mode at the internal current-generator (I-gen) plane and package plane are investigated, respectively, and a novel dual-band matching network topology is designed to simultaneously present required load impedances at the fundamental and harmonic impedances of both operation frequencies. First, a harmonic control network is designed to control the harmonic impedances precisely for CCF operation. Then, the fundamental impedances are synthesized using the real frequency technique. To verify the validity of proposed methodology, a dual-band CCF PA operating at 2.6 and 3.5 GHz is designed, fabricated, and measured. The measurement results show that the peak drain efficiency is 76.7% with an output power 42.4 dBm at the lower band and 72.8% with an output power 41.1 dBm at the upper band.

INDEX TERMS Continues Class-F, dual-band, harmonic control, high-efficiency, power amplifier, real frequency technique.

I. INTRODUCTION

The fast development of wireless communication systems and the roll-out of new standards require that the RF front can support multiple standards to meet the past and present demands of different industrial applications. Consequently, there is an increasing demand of broadband or multi-band RF components able to simultaneously manage different types of signals [1]–[3]. The power amplifier (PA) is a key component in broadband or multi-band system, since its performance strongly influence the overall system performance in terms of bandwidth, output power, and efficiency. Several different kinds of modes have been widely studied to improve the efficiency of the PA, such as Doherty PA [4], [5], Class-E [6], [7], Class-J [8] and Class-F [9]–[11]. To achieve high efficiency, harmonic impedances of the active

device need to be considered. The single operation mode might not satisfy the strict matching requirement at the entire operation band simultaneously, or the impedance solution spaces are very small, which limits the bandwidth of the PA. In this context, the continuous-mode PA such as continuous Class-B/J, continuous Class-F (CCF), continuous Class-F⁻¹ (CCF⁻¹) and series of continuous modes are consecutively proposed [12]–[17]. All these working modes provide practical theories and possibilities for designing broadband PAs.

The harmonic impedances should be precisely controlled to realize these high-efficiency modes. However, the performances of the broadband PAs are always ordinary as these harmonic impedances are not easy to be achieved in the whole designed band for broadband applications. Optimized designs for some target frequency bands might be more effective for

improving the performances of the PAs, especially when the different operation bands work at two arbitrary wide interval frequencies. Thus, multi-band PAs are also considered as the effective way for broadband or multi-band communication systems. Recently, concurrent dual-band PAs, as the simplest form of multi-band ones, have already been widely reported [18]–[20].

Dual-band matching technologies have also been presented in the literature recently to design dual-band PAs [21]–[28]. Fu *et al.* [21] showed a systematic approach for the design of a novel dual-band matching network, which mainly focused on the synthesis of fundamental frequency impedances, while harmonic impedances were tuned by adding a transmission line. A novel output network with harmonic control circuit up to third harmonic to realize dual-band PA was presented in [23], where also only tuning line was used to control the harmonic impedances. Dual-band unequal stepped impedance transformer was applied to match arbitrary complex-to-complex impedances at two arbitrary frequencies in [25], and subsequently the dual-band impedance transformer approach was proposed to design a matching network for a PA at two uncorrelated frequencies, while the harmonics impedances were neglected [26].

All of these proposed structures either not control the harmonic or not give the explicit analytical parameter expression of the harmonic, where the harmonic control was obtained only by tuning process. In the tuning approach, plenty of time will be spent to optimize the whole matching network as the tuning lines will affect the fundamental impedance matching. Another effective matching method is real frequency technique (RFT), which is widely used in broadband PA matching network design [29]–[31]. For example, commensurate stepped-impedance transmission lines were employed to design a broadband PA in [30], and shunt stubs were also employed for an ultra-wideband PA design in [31]. The design of matching network with RFT was only focused on the matching of fundamental impedances, and the harmonic impedances were not treated in these works.

In this paper, a novel structure with precise fundamental and harmonic control is proposed with a simple design procedure. With the proposed structure, an output matching network is presented to design a high-efficiency dual-band CCF PA. Firstly, a harmonic control network is designed to control the harmonic impedances precisely for CCF PA operation. Then, the fundamental impedances are synthesized effectively using the RFT.

This paper is organized as follows. In Section II, the optimal impedances of the CCF PA at internal current-generator (I-gen) plane and package plane are deduced, respectively. Based on the optimal impedances, the design of harmonic tuning and fundamental impedance matching network can be implemented separately to simplify the design process. A dual-band high-efficiency CCF PA at 2.6 GHz and 3.5 GHz with precise harmonic control is designed using the proposed design methodology. In Section III, the simulation and measurement results for the fabricated PA reveal that

drain efficiency greater than 70% is achieved at 2.6 GHz and 3.5 GHz with an output power 42.4 dBm and 41.1 dBm. Moreover, digital pre-distortion (DPD) technique is also used to improve the linearity of the PA. Conclusions are then given in Section IV.

II. DESIGN METHODOLOGY

A. OPTIMAL IMPEDANCES OF CCF PA MODE

The CCF mode of PA operation is an extension of the classical Class-F mode. This mode utilizes the concept of a series of optimal impedance solutions instead of a singular one, where constant open-circuit termination is at the third harmonic and short-circuit termination is at the second harmonic. The design space of this mode is extended while the output power and efficiency maintain unchanged compared with the traditional Class-F mode PA.

The intrinsic half-sinusoidal drain current waveform normalized to I_{max} , which is the same as Class-B/F mode, can be expressed as

$$i_{ds}(\theta) = \frac{1}{\pi} + \frac{1}{2} \cos(\theta) + \frac{2}{3\pi} \cos(2\theta) + \dots \quad (1)$$

The normalized drain voltage can be given by the extension of the Class-F voltage multiplying a factor $(1 - \gamma \sin(\theta))$

$$v_{ds}(\theta) = (1 - \frac{2}{\sqrt{3}} \cos(\theta) + \frac{1}{3\sqrt{3}} \cos(3\theta))(1 - \gamma \sin(\theta)) \quad -1 \leq \gamma \leq 1 \quad (2)$$

According to the current coefficients of (1) and the voltage components of (2), the optimal impedances up to the third harmonic can be obtained as:

$$Z_F = (\frac{2}{\sqrt{3}} + j^*(1 - \frac{7}{12\sqrt{3}}) \gamma)^* R_{opt} \quad (3a)$$

$$Z_{2F} = -j^* \frac{7\sqrt{3}\pi}{24} \gamma^* R_{opt} \quad (3b)$$

$$Z_{3F} = \infty \quad (3c)$$

$$R_{opt} = 2V_{dc}/I_{max} \quad (4)$$

Where R_{opt} is defined as the optimal fundamental impedance of Class-B PA with all harmonics short-circuit, V_{dc} and I_{max} represent the transistor drain-source dc-bias voltage and maximum transistor current, respectively. Based on (3a), the impedance at the fundamental frequency is varied, which can be viewed as a circle of constant resistance. The impedance at the second harmonic frequency remains purely reactive while the impedances at the third harmonic frequency are infinite at the I-gen plane of the device. This CCF operating mode can be applied to design the broadband PA.

In this work, GaN CGH40010F from Cree is chosen as the active device for designing the dual-band PA. As the existence of device output parasitic as well as the package, the theoretical impedance at the I-gen plane should be converted to that at the package plane. By employing the approximate parasitic equivalent network model demonstrated in [32], the optimal impedances at the package plane at 2.6 GHz and 3.5 GHz can be reassessed and displayed in Fig. 1.

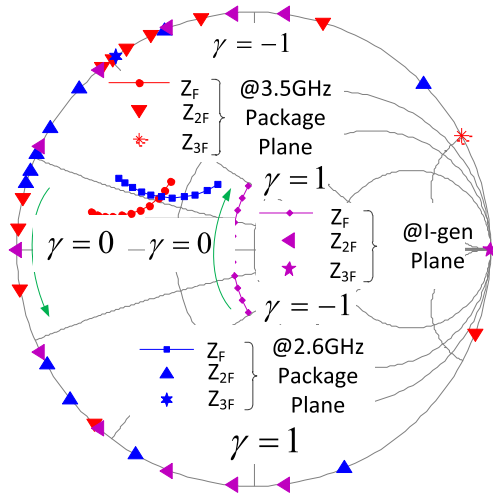


FIGURE 1. Theoretical fundamental, second harmonic, and third harmonic impedance at the I-gen plane and corresponding approximate impedance at the package plane.

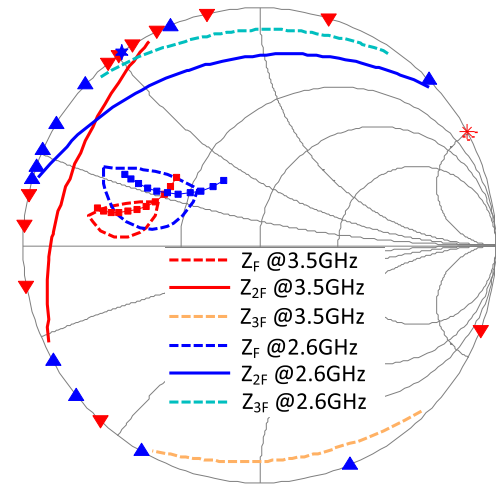


FIGURE 2. Merged output power and efficiency contours (drain efficiency > 75%, output power > 41dBm) for fundamental impedances at two operation frequencies and the optimum region for harmonic impedances (efficiency degradation less than 2%) extracted from the load-pull simulation.

On the other hand, the theoretical analysis results presented in Fig. 1 are based on the approximate parasitic model, and any deviation from the real device will impact the performances of the circuit. Therefore, to validate the effectiveness of the theoretical impedance and further improve the performance of the PA, load-pull simulations based on the nonlinear device with a large-signal model are carried out in ADS2013 to find the optimal fundamental and harmonic impedances. The merged output power and efficiency contours (drain efficiency > 75%, output power > 41 dBm) at two operation frequencies are presented in Fig. 2 and the optimum regions for second and third harmonic impedances are also given from the load-pull simulation results. It can be found that the optimum fundamental and second harmonic impedances obtained from load-pull simulations match well with those derived from the theoretical analysis based on the approximate parasitic model. The third harmonic at 2.6 GHz also agrees well with the theoretical result while the value at 3.5 GHz has a slight error, which may be caused by the inaccuracy of the large signal model at high frequency.

As for the input matching network, the source input impedance plays a less critical role for improvement of the PA performance. Thus, only the fundamental source impedance is considered and the harmonic impedances are neglected when designing the input matching network.

According to load-pull simulation results, the fundamental and harmonic impedances at $f_1 = 2.6$ GHz and $f_2 = 3.5$ GHz are given in Table 1. The design of the fundamental and harmonic impedances matching network will be carried out based on these impedance values.

B. DESIGN OF HARMONIC TUNING NETWORK

As investigated in the previous section, the design space for the fundamental and harmonic impedance at package plane has been obtained in the CCF mode, now the harmonic tuning

TABLE 1. Optimal impedance from load-pull simulation.

Impedance Frequency	Output optimal Impedance(Ω)	Input optimal impedance(Ω)
f_1	15.5+j*7.9	10.33-j*8.3
f_2	11.46+j*4.8	11.1-j*7.7
$2f_1$	j*25.9	none
$2f_2$	j*12	none
$3f_1$	j*63	none
$3f_2$	-j*118	none

and fundamental frequency matching can be considered separately in a simple design process. As an important part in the design of a PA, the harmonic tuning network should be realized firstly, and the proposed structure is shown in Fig. 3. This proposed network is composed of third harmonic control and second harmonic control circuit. The corresponding design process is to control these harmonic impedances precisely.

To start with, the harmonic tuning network is designed using the shunted quarter-wave transmission line (SQL) operation at the harmonic frequency, which is given in Fig. 3. As shown in the Figure, the SQL is used to introduce short circuit condition for the proper reference plane of the matching network, which is related to the harmonic frequencies to be controlled. The transmission lines T1, T2, T3 are used to design the third harmonic control network and T4, T5, T6 are used to design the second harmonic control network.

The lengths of the SQL can be determined by

$$\theta_{T2}^{@3f_1} = \theta_{T3}^{@3f_2} = 90^\circ \tag{5}$$

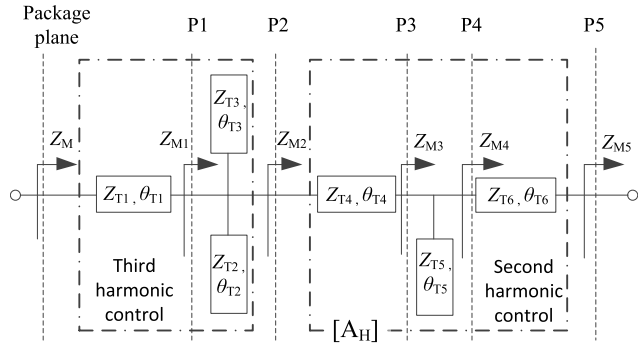


FIGURE 3. Schematic of the proposed harmonic tuning network using SQLs.

And the ratio of the two uncorrelated frequencies can be defined as:

$$f_2/f_1 = k \quad (6)$$

Then the following parameter k_i is defined to represent the ratio between the different fundamental and harmonic frequency f_i ($i = 1, 2, 3, 4, 5, 6$) and fundamental frequency f_1

$$k_i = \begin{cases} 1 & i = 1@f_1 \\ k & i = 2@f_2 \\ 2 & i = 3@f_3 = 2f_1 \\ 2k & i = 4@f_4 = 2f_2 \\ 3 & i = 5@f_5 = 3f_1 \\ 3k & i = 6@f_6 = 3f_2 \end{cases} \quad (7)$$

By introducing these parameters, all the electrical lengths calculated at f_1 will be convenient for calculating the impedances at different planes. Then the electrical lengths of the SQL can be calculated as

$$\theta_{T2} = \pi/2k_5 \quad (8)$$

$$\theta_{T3} = \pi/2k_6 \quad (9)$$

If short circuit conditions are satisfied at plane P1 in Fig. 3, the transmission line T1 can be used to control the impedances at $3f_1$ and $3f_2$, the impedances $Z_M(f_i)$ ($i = 5, 6$) can be calculated as:

$$Z_M(f_5) = j^* Z_{T1}^* \tan(k_5 \theta_{T1}) \quad (10)$$

$$Z_M(f_6) = j^* Z_{T1}^* \tan(k_6 \theta_{T1}) \quad (11)$$

Combining (10) and (11), the characteristic impedance Z_{T1} and electrical length θ_{T1} can be calculated out.

The characteristic impedances Z_{T2} and Z_{T3} are the free parameters for circuit design, which values will affect the impedances at plane P1. Moreover, to provide enough impedance values at the fundamental frequencies, the characteristic impedances of these transmission lines should be assigned with larger values.

Once the parameters of transmission line T1 are determined, the impedances $Z_M(f_i)$ ($i = 1, 2, 3, 4$) at plane

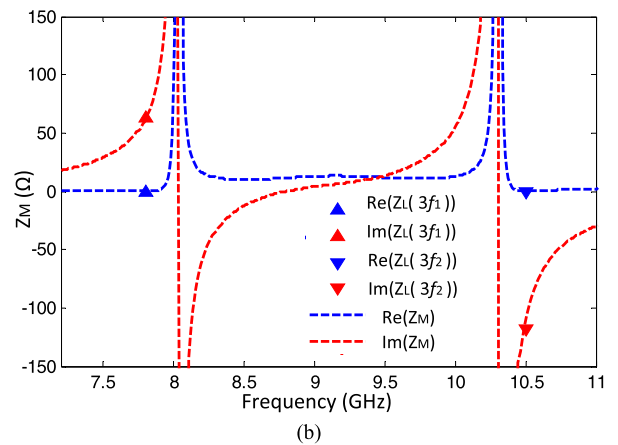
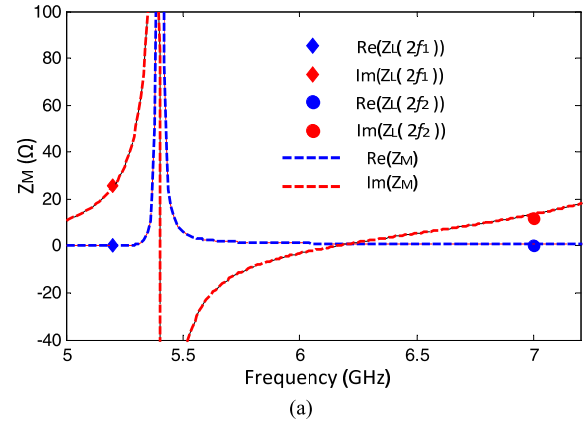


FIGURE 4. The input impedance of the harmonic tuning network versus frequency and the optimal harmonic impedance at package plane.

package plane are expressed as:

$$Z_M(f_i) = Z_{T1} \frac{Z_{M1}(f_i) + j^* Z_{T1}^* \tan(k_i \theta_{T1})}{Z_{T1} + j^* Z_{M1}(f_i)^* \tan(k_i \theta_{T1})} \quad (12)$$

By rearranging (12), the impedances $Z_{M1}(f_i)$ at plane P1 can be expressed as:

$$Z_{M1}(f_i) = Z_{T1} \frac{Z_M(f_i) - j^* Z_{T1}^* \tan(k_i \theta_{T1})}{Z_{T1} - j^* Z_M(f_i)^* \tan(k_i \theta_{T1})} \quad (13)$$

On the other hand, the impedances $Z_{M1}(f_i)$ can be easily inferred by the following relationship:

$$Z_{M1}(f_i) = Z_{M2}(f_i) // (-j \cdot Z_{T2} \cdot \cot(k_i \theta_{T2})) // (-j \cdot Z_{T3} \cdot \cot(k_i \theta_{T3})) \quad (14)$$

Combining (13) and (14), the impedances $Z_{M2}(f_i)$ ($i = 1, 2, 3, 4$) at plane P2 of Fig. 4 can be obtained.

Then, the electrical length of the SQL T5 can be expressed as:

$$\theta_{T5} = \pi/2k_3 \quad (15)$$

As the short circuit condition at $2f_1$ is satisfied at plane P3 of Fig. 4, if the characteristic impedance Z_{T4} is assumed to

be a free design parameter, then the electrical length θ_{T4} can be obtained as:

$$\theta_{T4} = \frac{1}{k_3} \arctan\left(\frac{Z_{M2}(f_3)}{j \cdot Z_{T4}}\right) \quad (16)$$

Similarly, the impedance $Z_{M3}(f_4)$ at plane P3 of Fig. 4 can be expressed as:

$$Z_{M3}(f_4) = Z_{T4} \frac{Z_{M2}(f_4) - j^* Z_{T4}^* \tan(k_4 \theta_{T4})}{Z_{T4} - j^* Z_{M2}(f_4)^* \tan(k_4 \theta_{T4})} \quad (17)$$

Then, considering the SQL T5, it is easy to obtain the equation of the impedance $Z_{M3}(f_4)$ at plane P1 as:

$$Z_{M3}(f_4) = Z_{M4}(f_4) // (-j \cdot Z_{T5} \cdot \cot(k_4 \theta_{T5})) \quad (18)$$

After rearranging (18), the relationship between $Z_{M3}(f_4)$ and $Z_{M4}(f_4)$ can be derived as:

$$Z_{M4}(f_4) = \frac{j \cdot Z_{M3}(f_4) \cdot Z_{T5} \cdot \cot(k_4 \theta_{T5})}{Z_{M3}(f_4) + j \cdot Z_{T5} \cdot \cot(k_4 \theta_{T5})} \quad (19)$$

Once the impedance at plane P4 is obtained, the transmission line T6 can be used to control the impedance at $2f_2$. On the other hand, the second harmonic impedance of f_2 at plane P5 is infinite as the fundamental matching network is designed with RFT, which mean that series open condition is satisfied. Then the impedance at P4 is

$$Z_{M4}(f_4) = -j^* Z_{T6}^* \cot(k_4 \theta_{T6}) \quad (20)$$

Assuming the characteristic impedance Z_{T6} is a free design parameter, the electrical length θ_{T6} can be obtained by

$$\theta_{T6} = \frac{1}{k_4} \arccot\left(\frac{j \cdot Z_{M4}(f_4)}{Z_{T6}}\right) \quad (21)$$

As a result, the transmission line T3 as well as T1 and T2 can be used to control the second harmonic impedances.

Up to now, the electrical lengths θ_{T1} , θ_{T2} , θ_{T3} , θ_{T4} , θ_{T5} , θ_{T6} , and Z_{T1} are all calculated out. It should be noted that the characteristic impedances Z_{T2} , Z_{T3} , Z_{T4} , Z_{T5} , and Z_{T6} are all free design parameters, which can give larger design spaces for harmonic control as well as fundamental matching. Consequently, these values can be selected in a large range, which can fit the physical constrains on the adopted technology or decrease the network size.

According to the harmonic impedances from the load-pull simulations in the previous section, the parameters of the harmonic structure are given in Table 2. The simulation results of the harmonic tuning network are shown in Fig. 4.

TABLE 2. Calculation results of the harmonic tuning network.

θ_{T1} (deg)	θ_{T2} (deg)	θ_{T3} (deg)	θ_{T4} (deg)
24.6	30	22.3	91
θ_{T5} (deg)	θ_{T6} (deg)	Z_{T1} (Ω)	Z_{T2} (Ω)
45	38	18.1	80
Z_{T3} (Ω)	Z_{T4} (Ω)	Z_{T5} (Ω)	Z_{T6} (Ω)
80	42	45	40

It can be seen from Fig.4 that the second and third harmonic impedances are precisely controlled.

C. FUNDAMENTAL MATCHING WITH RFT

Once the harmonic tuning network is designed, the ABCD-parameters of this network can be derived by applying a matrix formulation of cascaded two-port networks, which can be given as

$$[A_{Hi}] = \begin{bmatrix} \cos(k_i \theta_{T4}) & jZ_{T4} \sin(k_i \theta_{T4}) \\ \frac{j \sin(k_i \theta_{T4})}{Z_{T4}} & \cos(k_i \theta_{T4}) \end{bmatrix} \cdot \begin{bmatrix} 1 & 0 \\ \frac{j \tan(k_i \theta_{T5})}{Z_{T5}} & 1 \end{bmatrix} \cdot \begin{bmatrix} \cos(k_i \theta_{T6}) & jZ_{T6} \sin(k_i \theta_{T6}) \\ \frac{j \sin(k_i \theta_{T6})}{Z_{T6}} & \cos(k_i \theta_{T6}) \end{bmatrix} = \begin{bmatrix} A_i & B_i \\ C_i & D_i \end{bmatrix} \quad (22)$$

The fundamental impedances at plane P4 of Fig.3 can be rewritten as:

$$Z_{M5}(f_i) = \frac{Z_{M2}(f_i) \cdot D_i - B_i}{A_i - Z_{M2}(f_i) \cdot C_i} \quad (23)$$

Then these impedances at plane P5 of Fig.3 can be obtained as $Z_{M5}(f_1) = 6.2 + j^*8.7$ and $Z_{M5}(f_2) = 3 - j^*19$. As these impedances are obtained, the next important step is to design the matching network. Dual-band matching technologies have been reported in [25]–[28], where topological structures are always chosen first and then the parameters are deduced by complex formula derivations and tedious calculations. The RFT is a numerical optimization algorithm used for the synthesis of passive networks, where commensurate transmission lines are used to realize the matching network. In recent years, this technique is widely used for broadband PA matching network design [22], [24], [29]–[31].

As described in [33], The Richard variable can be defined as follows:

$$\lambda = j^* \tan(w\tau) = j^* \tan\left(\frac{wl}{v_p}\right) \quad (24)$$

Where τ is the constant delay, l is the length of the commensurate transmission lines, and v_p is the velocity of the wave propagation within the medium. The length of the commensurate transmission line is $l = \lambda_0/8^* \gamma$, where λ_0 represents the wavelength at the higher frequency 3.5 GHz of the operation frequencies and the variable γ is used to control the length of the commensurate transmission line. It should be noted that $\gamma = 1$ is assigned to ensure the open condition of the second harmonic impedance of 3.5 GHz.

Now, the impedance composed of commensurate transmission lines can be expressed using a positive-real, rational function

$$Z_{M5}(\lambda) = \frac{N(\lambda)}{D(\lambda)} = \frac{a_m \lambda^m + a_{m-1} \lambda^{m-1} + \dots + a_1 \lambda^1 + a_0}{b_n \lambda^n + b_{n-1} \lambda^{n-1} + \dots + b_1 \lambda^1 + b_0} \quad (25)$$

This function is also called driving point function (DPF), which can be used to represent the input impedances at different frequencies. Once the DPF is obtained, the next step is to synthesize the DPF with commensurate transmission lines.

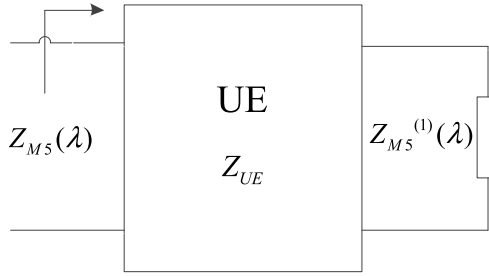


FIGURE 5. Relation among initial and remaining DPF after removal of a UE.

A unit element (UE) with characteristic impedance $Z_{M5}(1)$ can be removed from a DPF at any time. The relation between initial DPF and remaining DPF after removal of an UE is given in Fig. 5, where $Z_{M5}(\lambda)$ is the original DPF and $Z_{M5}^{(1)}(\lambda)$ is the remaining DPF. The remaining DPF can be expressed as follows [31]

$$Z_{M5}^{(1)}(\lambda) = Z_{M5}(1) \frac{Z_{M5}(\lambda) - \lambda Z_{M5}(1)}{-\lambda Z_{M5}(\lambda) + Z_{M5}(1)} \quad (26)$$

In this paper, the initial DPF can be obtained after optimization, which can be given as follows:

$$Z_{M5}(\lambda) = \frac{0.02349\lambda^4 + 7.34871\lambda^3 + 4.91509\lambda^2 + 2.41699\lambda + 1}{0.85137\lambda^4 + 0.58239\lambda^3 + 0.64967\lambda^2 + 0.34256\lambda + 0.02} \quad (27)$$

Four UEs have been applied to optimize the DPF, correspondingly, four times of UE extraction should be used to synthesize the DPF.

A UE with characteristic impedance $Z_{UE1} = Z_{M5}(1) = 6.4$ is first removed and the remaining DPF is

$$Z_{M5}^{(1)}(\lambda) = \frac{5.46613\lambda^3 + 3.71569\lambda^2 + 2.28858\lambda + 1}{0.003659\lambda^3 + 0.29322\lambda^2 + 0.18681\lambda + 0.02} \quad (28)$$

Then, a UE with characteristic impedance $Z_{UE2} = Z_{M5}^{(1)}(1) = 24.8$ is removed for the second time, and the remaining DPF is

$$Z_{M5}^{(2)}(\lambda) = \frac{0.090587\lambda^2 + 1.79342\lambda + 1}{0.22078\lambda^2 + 0.14642\lambda + 0.02} \quad (29)$$

Again, a UE with characteristic impedance $Z_{UE3} = Z_{M5}^{(2)}(1) = 7.5$ is removed for the third time, which resulting in the following DPF

$$Z_{M5}^{(3)}(\lambda) = \frac{1.64445\lambda + 1}{0.012162\lambda + 0.02} \quad (30)$$

Finally, a UE with $Z_{UE4} = Z_{M5}^{(3)}(1) = 82.2$ is removed and the network is ended with a resistor $R_{load} = 50$.

The characteristic impedances of the transmission lines are given in Fig. 6. The electric length is 45° at 3.5 GHz. The simulation results of the synthesized impedance versus frequency are shown in Fig.7. It can be seen that the desired impedances at two operation frequencies are well matched.

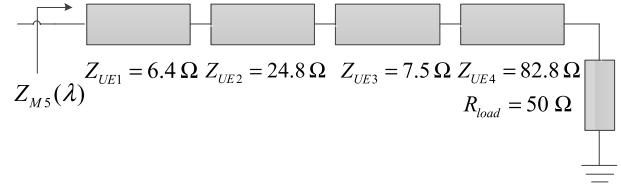


FIGURE 6. The parameters of the synthesized fundamental output matching network with RFT.

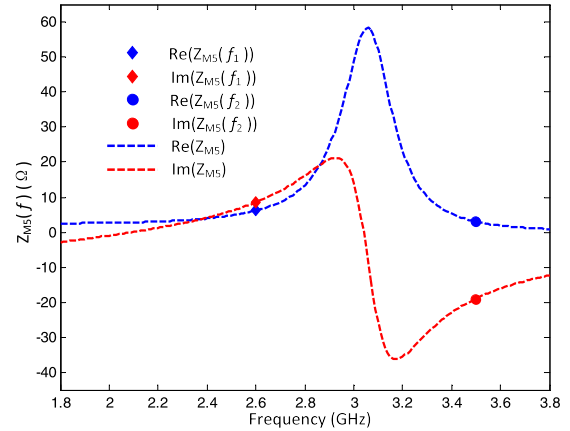


FIGURE 7. The synthesized input impedance versus frequency and required fundamental impedance at Plane 5.

The separated design of fundamental matching and harmonic turning network simplifies the difficulty of matching network design. Meanwhile, as the SQL is used to introduce short circuit condition at the specified reference plane of the harmonic turning network, the design of the fundamental matching network will not affect the harmonic matching network. This gives a more precise harmonic control approach, which is important for CCF mode and is convenient to design the following fundamental matching network. And also RFT is a effective method for designing the dual-band fundamental matching network. This novel separated design structure is suitable for fundamental matching and precise harmonic control network design.

As for the design of the input matching network, the fundamental source impedance is considered and the harmonic impedances are neglected. Hence, to guarantee a precise impedance matching at the interesting operation band, four UEs are used to design the input matching network. The DPF of the input matching network can be given as follows:

$$Z_{input}(\lambda) = \frac{0.24426\lambda^4 + 1.80033\lambda^3 + 3.50957\lambda^2 + 2.39799\lambda + 1}{0.08188\lambda^4 + 0.23947\lambda^3 + 0.26107\lambda^2 + 0.17151\lambda + 0.02} \quad (31)$$

The synthesis method of the input matching network is the same as the output matching network. The details will be not presented in here again. The complete circuit layout of the PA is shown in Fig. 8. The power supply line is inserted into the

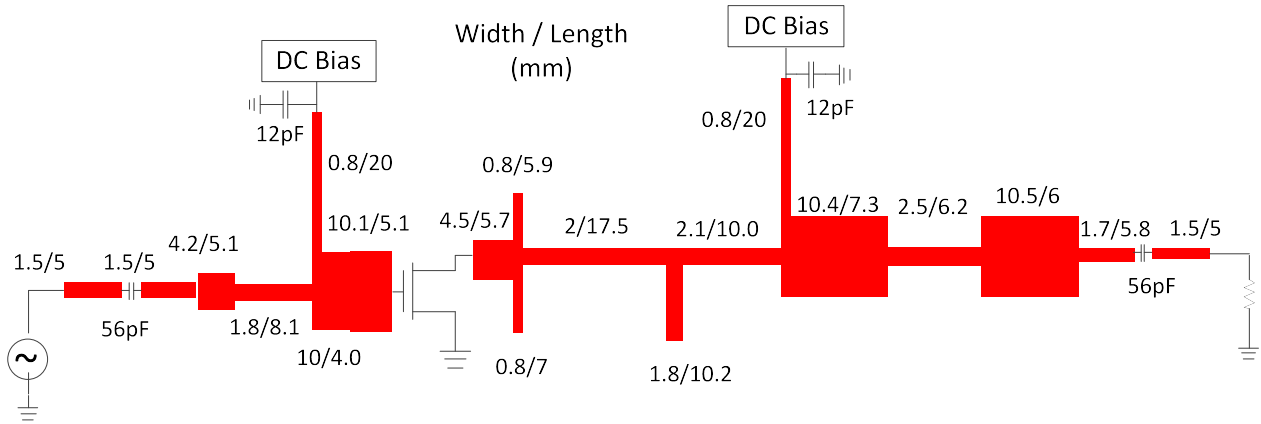


FIGURE 8. Layout of the complete PA circuit.

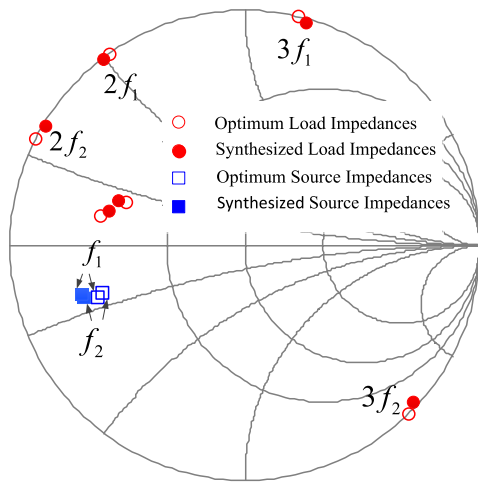


FIGURE 9. Comparisons between the synthesized impedances and the optimum impedances at two operation frequencies.

matching network and the discontinuities between adjacent elements have been taken into consideration. Some of the optimization steps are also required to eliminate these effects. The electromagnetic (EM) simulation results of the synthesized matching network and the optimum load impedances are presented in Fig. 9. These results show that good matching is achieved at both fundamental and harmonic impedances.

In summary, the detailed design steps for design of the dual-band PA can be given as follows.

- 1) Deducing the optimal impedance at I-gen plane and package plane according to the operation PA CCF mode and de-embedding technology, and finding out the design spaces for the fundamental and harmonic impedances based on load-pull simulation.
- 2) Firstly, the third harmonic matching network and second harmonic matching network can be designed by applying the SQLs with (6)-(21).
- 3) Calculating the fundamental impedance at plane P5 with the ABCD parameters of the harmonic

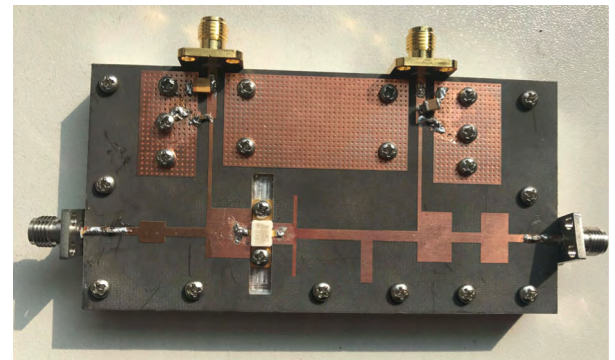


FIGURE 10. Photograph of the fabricated PA.

matching network (22) and (23), and designing the fundamental matching network with RFT separately.

- 4) Designing the input matching network with RFT.
- 5) Some optimization steps are carried out for improving the circuit performance.

Applying these steps, a high performance dual-band CCF PA can be designed straightforward.

III. SIMULATION AND EXPERIMENTAL TESTS

A. CONTINUOUS-WAVE (CW) MEASUREMENTS

The proposed PA is realized on the Rogers 5880 substrate with $\epsilon_r = 2.2$ and $H = 20$ mil. The fabricated dual-band PA is given in Fig. 10. To verify the operating mode of the designed PA, the voltage and current waveforms at I-gen plane are simulated at 2.6 GHz and 3.5 GHz in ADS prior to measurement, which are given in Fig. 11(a)-(b). As can be seen from Fig. 11, the currents are similar to that of standard CCF PAs while the voltages are a little different from the ideal ones, this may be caused by the finite harmonic control and inaccurate approximate parasitic model of the active device. While the overlapped areas of voltage and current are quite small, which indicate that high efficiency mode can be achieved in the corresponding operation frequencies.

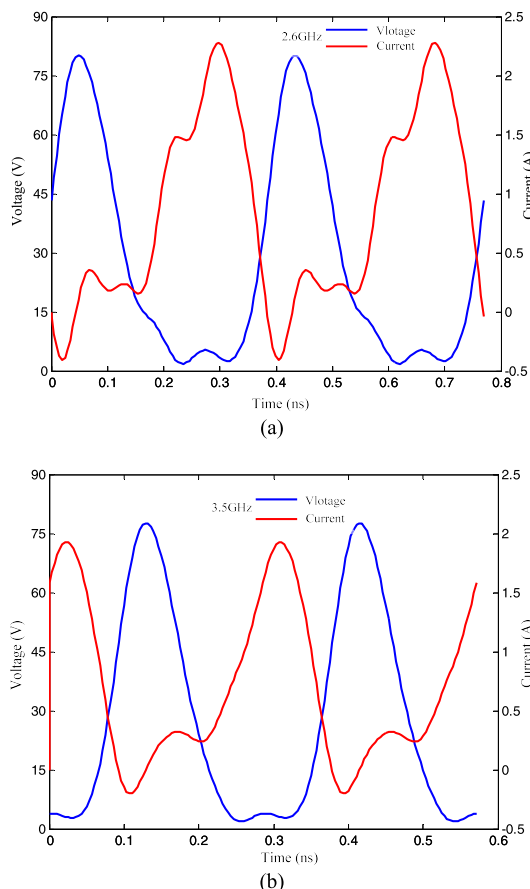


FIGURE 11. De-embedded voltage and current waveforms of the PA at I-gen plane. (a) 2.6GHz. (b) 3.5GHz.

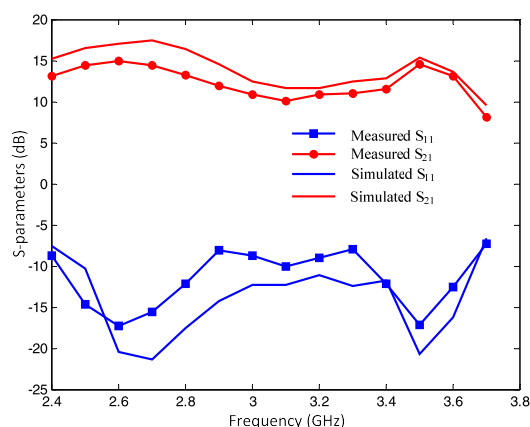


FIGURE 12. Simulated and measured S-parameters of the PA versus frequency.

Fig. 12 shows the simulated and measured small signal S-parameters of the fabricated dual-band PA using ADS and Agilent network analyzer E5063A respectively. Measured return losses are better than 16 dB in 2.6 GHz and 3.5 GHz. And the measured gains are about 15 dB at the operation frequencies.

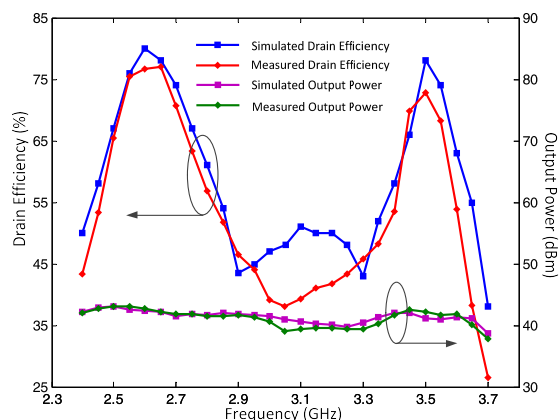


FIGURE 13. Simulated and measured DE and output power versus frequency in the operation band from 2.4-3.7 GHz.

The single-tone CW signal measurements are first performed at 2.6 GHz and 3.5 GHz. The gate of the transistor is biased at -2.8 V and the drain bias is 28 V in the measurement setup. Agilent E4433B signal generator is used to generate the test signal and Agilent N9010A EXA signal analyzer is used to measure the PA output power. A broadband linear driver PA is also used to pre-amplify the signal and a 20 dB attenuator is connected after fabricated PA to protect the signal analyzer. Measured and simulated results of drain efficiency (DE) and output power vary with frequency are given in Fig. 13. It can be seen that the DE is over 60% throughout the bandwidth from 2.5 GHz to 2.75 GHz and over 65% from 3.45 GHz to 3.55 GHz. The maximum DE is 76.7% occurred at 2.6 GHz, and the measured output power is 42.4 dBm and 41.1 dBm, corresponding to 17.4 W and 12.8 W at 2.6 GHz and 3.5 GHz. It should be noted that the DE performance outside the operation frequency band has little degradation, which may be caused by the inaccurate model of the packaged transistors and the errors of fabrication. Fig. 14 shows the measured DE and gain versus output power at two operation frequencies. It can be seen that the saturated gain is 11.5 dB at 2.6 GHz and 10.5 dB at 3.5 GHz. The DE can reach 76.7% at 2.6 GHz with an output power 42.4 dBm and 72.8% at 3.5 GHz with an output power 41.1 dBm. Moreover, the maximum output powers of 39.6 dBm and 38.2 dBm are obtained at 2.6 GHz and 3.5 GHz in the concurrent mode. It is also shown that maximum concurrent mode DE is up to 61.6%, which is lower than those in the single-tone mode.

A summary of some similar published dual-band PAs is given in Table 3. The comparisons show that the proposed PA can achieve almost the best DE performance considering power level and operation frequency. It demonstrates that the proposed matching method is very effective for designing the matching network with precise harmonic control, which is useful for the design of high efficiency dual-band PAs.

B. LTE MODULATED-SIGNAL MEASUREMENTS

To evaluate the performance of the PA for modulated signal in modern wireless communication systems, the designed

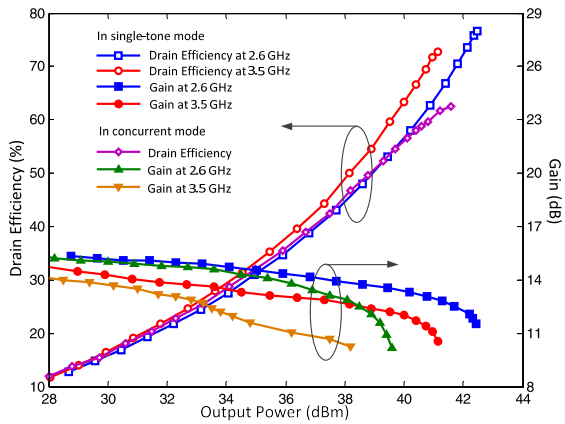


FIGURE 14. Measured drain efficiency and gain versus output power at 2.6 GHz and 3.5 GHz.

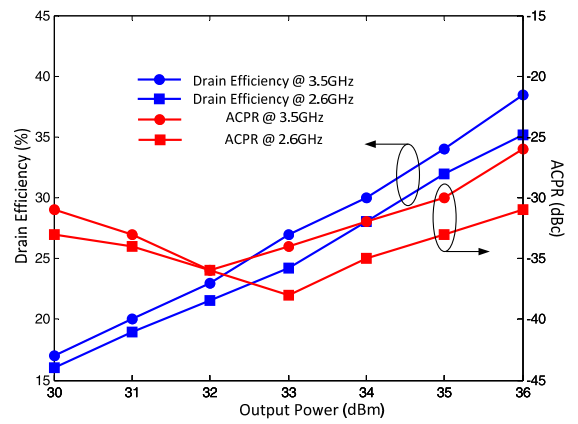


FIGURE 15. Measured ACPR and drain efficiency versus output power at 2.6 and 3.5GHz using a 5MHz LTE signal with PAPR=7.5dB.

TABLE 3. Compared with reported dual-band PAs.

Ref. (Year)	Frequency (GHz)	Pout (W)	DE (%)	Gain (dB)	Matching Method
[19] (2008)	2.45/3.3	33/32.5	53/46	7/5	topology and harmonic turning
[25] (2011)	1.96/3.5	40/40	60/55	14/11	dual-band transformer
[20] (2013)	1.9/2.6	41.5/41.5	76/70	11/11	analysis and topology
[21] (2014)	0.8/1.9	46/46	68/68	not given	topology
[22] (2015)	2.4/3.45	41.7/41.5	69.4/70.7	12.7/10.5	RFT
[23] (2016)	1.9/2.6	41.1/40.8	80/74	10/10	topology and harmonic turning
[24] (2017)	2.35/3.45	40.6/41.2	70.3/71.4	10.6/11.2	analysis and RFT
This work	2.6/3.5	42.4/41.1	76.7/72.8	11.5/10.5	harmonic turning and RTF

PA is tested using the modulated 5-MHz LTE signals with PAPR of 7.5 dB. Fig. 15 shows the measured drain efficiency and the adjacent channel power ratio (ACPR) versus output power at two different frequencies. As can be seen, with the increment of output power from 30 dBm to 36 dBm, the DE gradually increases to 35.5%, while ACLR is between -31.2 dBc and -38 dBc at 2.6 GHz and the DE gradually increases to 38%, while ACLR is between -25.5 dBc and -35 dBc at 3.5 GHz. The normalized power spectral of the PA with and without digital predistortion (DPD) are displayed in Fig. 16. The output power is about 36 dBm with DE of 35.2% at 2.6 GHz and 35 dBm with DE of 34.5% at 3.5 GHz. Better than -50 dBc ACPR is obtained after DPD, more than 20-dB improvement can be achieved compared to the original -30 dBc ACPR values at the two operation frequencies.

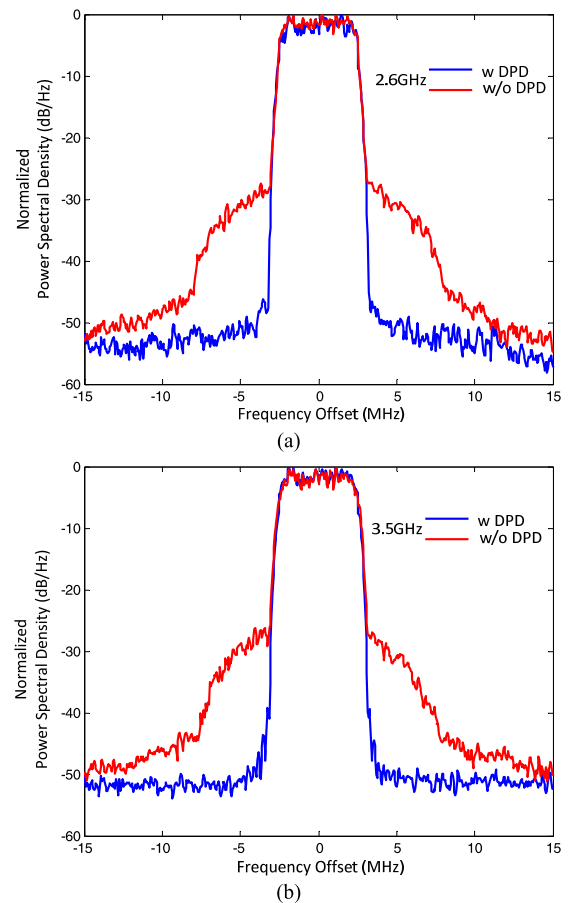


FIGURE 16. Measured normalized power spectral density with and without DPD using 5MHz LTE signals with PAPR=7.5dB. (a) 2.6GHz. (b) 3.5GHz.

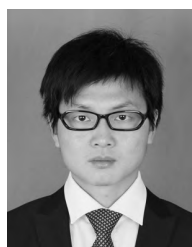
IV. CONCLUSION

A methodology for designing a high-efficiency concurrent dual-band CCF PA has been presented in this paper. To maintain high efficiency performances over the operation frequencies, the fundamental and harmonic impedances should be carefully controlled. CCF mode is adopted to expand the

design spaces of the impedances. The harmonic tuning and fundamental impedance matching networks are designed separately, which can result in a simple design process. Harmonic impedances up to third order are controlled precisely with SQL approach and the fundamental impedances are matched well by applying RFT. A 2.6 / 3.5 GHz dual-band CCF PA is then designed using a commercial 10-W GaN transistor to verify the proposed matching method. The proposed dual-band PA can achieve 76.7% and 72.8% drain efficiency at 2.6 GHz and 3.5 GHz. The corresponding output power is 42.4 dBm and 41.1 dBm. Measurement with 5-MHz LTE signals reveals that better than -50 dBc ACPR is obtained after DPD compared to the original ACPR of PA output signals.

REFERENCES

- [1] H. Hu and S. V. Georgakopoulos, "Multiband and broadband wireless power transfer systems using the conformal strongly coupled magnetic resonance method," *IEEE Trans. Ind. Electron.*, vol. 64, no. 5, pp. 3595–3607, May 2017.
- [2] D. Kalim and R. Negra, "Concurrent planar multiharmonic dual-band load coupling network for switching-mode power amplifiers," in *IEEE MTT-S Int. Microw. Symp. Dig.*, Jun. 2011, pp. 1–4.
- [3] K. Rawat, M. S. Hashmi, and F. M. Ghannouchi, "Dual-band RF circuits and components for multi-standard software defined radios," *IEEE Circuits Syst. Mag.*, vol. 12, no. 1, pp. 12–32, Feb. 2012.
- [4] V. Camarchia, M. Pirola, R. Quaglia, S. Jee, Y. Cho, and B. Kim, "The Doherty power amplifier: Review of recent solutions and trends," *IEEE Trans. Microw. Theory Techn.*, vol. 63, no. 2, pp. 559–571, Feb. 2015.
- [5] C. Huang, S. He, and F. You, "Design of broadband modified class-J Doherty power amplifier with specific second harmonic terminations," *IEEE Access*, vol. 6, pp. 2531–2540, 2018.
- [6] A. Grebennikov, "High-efficiency class-E power amplifier with shunt capacitance and shunt filter," *IEEE Trans. Circuits Syst. I, Reg. Papers*, vol. 63, no. 1, pp. 12–22, Sep. 2016.
- [7] M. Fu, H. Yin, M. Liu, and C. Ma, "Loading and power control for a high-efficiency class E PA-driven megahertz WPT system," *IEEE Trans. Ind. Electron.*, vol. 63, no. 11, pp. 6867–6876, Nov. 2016.
- [8] P. Wright, J. Lees, J. Benedikt, P. J. Tasker, and S. C. Cripps, "A methodology for realizing high efficiency class-J in a linear and broadband PA," *IEEE Trans. Microw. Theory Techn.*, vol. 57, no. 12, pp. 3196–3204, Dec. 2009.
- [9] M. Yang, J. Xia, Y. Guo, and A. Zhu, "Highly efficient broadband continuous inverse class-F power amplifier design using modified elliptic low-pass filtering matching network," *IEEE Trans. Microw. Theory Techn.*, vol. 64, no. 5, pp. 1515–1525, May 2016.
- [10] P. Colantonio, F. Giannini, G. Leuzzi, and E. Limiti, "On the class-F power amplifier design," *Int. J. RF Microw. Comput.-Aided Eng.*, vol. 9, no. 2, pp. 129–149, Feb. 1999.
- [11] T. Sharma et al., "High-efficiency input and output harmonically engineered power amplifiers," *IEEE Trans. Microw. Theory Techn.*, vol. 66, no. 2, pp. 1002–1014, Feb. 2018.
- [12] J. Chen, S. He, F. You, R. Tong, and R. Peng, "Design of broadband high-efficiency power amplifiers based on a series of continuous modes," *IEEE Microw. Wireless Compon. Lett.*, vol. 24, no. 9, pp. 631–633, Sep. 2014.
- [13] C. Friesicke, R. Quay, and A. Jacob, "The resistive-reactive class-J power amplifier mode," *IEEE Microw. Wireless Compon. Lett.*, vol. 25, no. 10, pp. 666–668, Oct. 2015.
- [14] T. Sharma, R. Darraji, F. Ghannouchi, and N. Dawar, "Generalized continuous class-f harmonic tuned power amplifiers," *IEEE Microw. Wireless Compon. Lett.*, vol. 26, no. 3, pp. 213–215, Mar. 2016.
- [15] S. Zheng, Z. Liu, X. Zhang, X. Zhou, and W. Chan, "Design of ultrawideband high-efficiency extended continuous class-F power amplifier," *IEEE Trans. Ind. Electron.*, vol. 65, no. 6, pp. 4661–4669, Jun. 2018.
- [16] T. Sharma, R. Darraji, and F. M. Ghannouchi, "A methodology for implementation of high efficiency broadband power amplifiers with second harmonic manipulation," *IEEE Trans. Circuits Syst. II, Exp. Briefs*, vol. 63, no. 1, pp. 54–58, Jan. 2016.
- [17] Y. Dong, L. Mao, and S. Xie, "Extended continuous inverse class-F power amplifiers with class-AB bias conditions," *IEEE Microw. Wireless Compon. Lett.*, vol. 27, no. 4, pp. 368–370, Apr. 2017.
- [18] K. Rawat and F. M. Ghannouchi, "Design methodology for dual-band Doherty power amplifier with performance enhancement using dual-band offset lines," *IEEE Trans. Ind. Electron.*, vol. 59, no. 12, pp. 4831–4842, Dec. 2012.
- [19] P. Colantonio, F. Giannini, R. Giofrè, and L. Piazzon, "A design technique for concurrent dual-band harmonic tuned power amplifier," *IEEE Trans. Microw. Theory Techn.*, vol. 56, no. 11, pp. 2545–2555, Nov. 2008.
- [20] X. Chen, W. Chen, F. M. Ghannouchi, Z. Feng, and Y. Liu, "Enhanced analysis and design method of concurrent dual-band power amplifiers with intermodulation impedance tuning," *IEEE Trans. Microw. Theory Techn.*, vol. 61, no. 12, pp. 4544–4558, Dec. 2013.
- [21] X. Fu, D. T. Bespalko, and S. Boumaiza, "Novel dual-band matching network for effective design of concurrent dual-band power amplifiers," *IEEE Trans. Circuits Syst. I, Reg. Papers*, vol. 61, no. 1, pp. 293–301, Jan. 2014.
- [22] Z. Dai, S. He, J. Pang, and C. Huang, "Semi-analytic design method for dual-band power amplifiers," *Electron. Lett.*, vol. 51, no. 17, pp. 1336–1337, Aug. 2015.
- [23] J. Pang, S. He, C. Huang, Z. Dai, C. Li, and J. Peng, "A novel design of concurrent dual-band high efficiency power amplifiers with harmonic control circuits," *IEEE Microw. Wireless Compon. Lett.*, vol. 26, no. 2, pp. 137–139, Feb. 2016.
- [24] Z. Dai, S. He, J. Pang, J. Peng, C. Huang, and F. You, "Sub-optimal matching method for dual-band class-J power amplifier using real frequency technique," *IET Microw., Antennas Propag.*, vol. 11, no. 9, pp. 1218–1226, 2017.
- [25] Y. Wu, Y. Liu, and S. Li, "A dual-frequency transformer for complex impedances with two unequal sections," *IEEE Microw. Wireless Compon. Lett.*, vol. 19, no. 2, pp. 77–79, Feb. 2009.
- [26] K. Rawat and F. M. Ghannouchi, "Dual-band matching technique based on dual-characteristic impedance transformers for dual-band power amplifiers design," *IET Microw., Antennas Propag.*, vol. 5, no. 14, pp. 1720–1729, Nov. 2011.
- [27] O. Manoochchri, A. Asoodeh, and K. Forooghi, "Pi-model dual-band impedance transformer for unequal complex impedance loads," *IEEE Microw. Wireless Compon. Lett.*, vol. 25, no. 4, pp. 238–240, Apr. 2015.
- [28] M. Chuang and M. Wu, "Transmission zero embedded dual-band impedance transformer with three shunt stubs," *IEEE Microw. Wireless Compon. Lett.*, vol. 27, no. 9, pp. 788–790, Sep. 2017.
- [29] D. Y.-T. Wu, F. M. Kadem, and S. Boumaiza, "Design of a broadband and highly efficient 45 W GaN power amplifier via simplified real frequency technique," in *IEEE MTT-S Int. Microw. Symp. Dig.*, May 2010, pp. 1090–1093.
- [30] N. Tuffy, L. Guan, A. Zhu, and T. J. Brazil, "A simplified broadband design methodology for linearized high-efficiency continuous class-F power amplifiers," *IEEE Trans. Microw. Theory Techn.*, vol. 60, no. 6, pp. 1952–1963, Jun. 2012.
- [31] Z. Dai, S. He, F. You, J. Peng, P. Chen, and L. Dong, "A new distributed parameter broadband matching method for power amplifier via real frequency technique," *IEEE Trans. Microw. Theory Techn.*, vol. 63, no. 2, pp. 449–458, Feb. 2015.
- [32] P. J. Tasker and J. Benedikt, "Waveform inspired models and the harmonic balance emulator," *IEEE Microw. Mag.*, vol. 12, no. 2, pp. 38–54, Apr. 2011.
- [33] M. Sengul, "Synthesis of cascaded lossless commensurate lines," *IEEE Trans. Circuits Syst. II, Exp. Briefs*, vol. 55, no. 1, pp. 89–91, Jan. 2008.



ZHENXING YANG received the B.Sc. degree in electronic engineering from the Nanjing University of Science and Technology, Nanjing, China, in 2014. He is currently pursuing the Ph.D. degree with the School of Microelectronics and Communication Engineering, Chongqing University, Chongqing, China.

His research interests include microwave and millimeter-wave devices and circuits, and wide-band high efficiency power amplifier design.



YAO YAO received the M.S. degree from the School of Electronic Engineering, Chengdu University of Technology, Sichuan, China, in 2011. She is currently pursuing the Ph.D. degree with the School of Electronic Science and Engineering, University of Electronic Science and Technology of China, Chengdu, China.

She is currently with the Smart Hybrid Radio Laboratory, University of Electronic Science and Technology of China. Her current research interests include digital predistortion techniques and software-defined radio.



TIAN LI received the B.Sc. degree in electronic engineering from the School of Microelectronics and Communication Engineering, Chongqing University, Chongqing, China, in 2017, where he is currently pursuing the Ph.D. degree.

His research interests include microwave and millimeter-wave circuits design, and high efficiency switchmode power amplifier design.



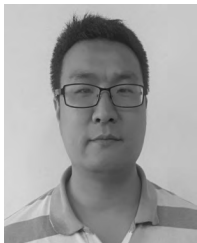
MINGYU LI received the Ph.D. degree in electronic engineering from the University of Electronic Science and Technology of China, Chengdu, China, in 2009. From 2012 to 2013, he was a Research Fellow with The University of Kitakyushu.

He is currently an Associate Professor with the School of Microelectronics and Communication Engineering, Chongqing University, Chongqing, China. His current research interests include RF/microwave transceiver design, statistical and adaptive signal processing for wireless communications, and behavioral modeling and linearization for RF power amplifiers.



ZHEN GENG received the B.Sc. degree in electronic engineering from the Chongqing University of Posts and Telecommunications, Chongqing, China, in 2017. She is currently pursuing the master's degree with the School of Microelectronics and Communication Engineering, Chongqing University, Chongqing.

Her research interests include communication signal processing and digital predistortion.



YI JIN received the B.E. degree in communication and information engineering from the Nanjing University of Information Science and Technology, Nanjing, China, in 2005, and the Ph.D. degree in communication and information engineering from Southeast University, Nanjing, in 2013. He is currently with the Xi'an Branch of the China Academy of Space Technology, Xi'an, China. His research interests include communication signal processing, satellite communication,

and networking.



ZHIQIANG YU received the B.Sc. degree in electronic engineering from Nanchang HangKong University, Nanchang, China, in 2017. He is currently pursuing the master's degree with the School of Microelectronics and Communication Engineering, Chongqing University, Chongqing, China.

His research interests include communication signal processing and digital predistortion implementation in FPGA.

...